Adsorption of Bromobenzene on Periodically Stepped and Nonstepped NiO(100)

Sarah C. Petitto, Erin M. Marsh, and Marjorie A. Langell*

Department of Chemistry, University of Nebraska, Lincoln, Nebraska 68588-0304

Received: July 12, 2005; In Final Form: October 15, 2005

Periodically stepped NiO(100) surfaces were prepared and characterized with low-energy electron diffraction (LEED), Auger electron spectroscopy (AES), X-ray photoelectron spectroscopy (XPS), and temperature-programmed desorption (TPD). Two vicinal NiO(100) single-crystal samples were cut, oriented, and polished with regular, repeating monatomic steps in six-atom or seven-atom terrace widths. LEED diffraction patterns showed characteristic spot-splitting that corresponded to the appropriate terrace and step height. The nonstepped and stepped NiO(100) surfaces were exposed to bromobenzene at 130 K first to produce a molecularly adsorbed monolayer species and then, with increased exposure, a multilayer adsorbate. An additional adsorbate species, observed only on the stepped surfaces, was found to desorb at 145 K by two competing pathways. One pathway, which saturates at low coverages, leaves bromine behind on the substrate and results in dehalogenation. The other pathway yields molecular desorption at 145 K, but is only observed in detectable amounts after the dehalogenation pathway is saturated. On both stepped and nonstepped NiO(100) substrates, adsorbed bromine resulting from dehalogenation processes appears as nickel bromide, determined by the Br 3p XPS data.

1. Introduction

Defects are often a controlling factor in the chemical reactivity of metal oxide surfaces[1−6] and are mechanistically important in partial oxidation catalysis, oxygen electrode and fuel cell technology, oxygen gas sensors, and other heterogeneous surface processes. A range of surface defect types is typically found on the substrate of any solid material under a given set of surface preparation conditions, no matter how carefully the surface has been prepared. Defects may be present in fairly low levels, but yet still play a substantial role in the surface chemistry of the solid. Isolating a particular type of defect for analysis and subsequent study in surface chemistry often proves impractical for many defect-laden surface structures. One method for modeling low-coordinate transition metal oxide defect species is using vicinally cut orientations that produce periodic step arrays.

We have modeled surface defects for NiO(100) with single-crystal substrates vicinally cut by 9.5° and 8.1° along ⟨010⟩ to produce periodic monatomic steps with six-atom and seven-atom terraces, respectively, of the nonpolar parent (100) plane. Vicinally cut surfaces with periodic step arrays have been produced for a number of metal substrates; however, studies reported for stepped transition metal oxide surfaces have focused primarily on naturally occurring, isolated step defects.[7−10] The earliest reference to the deliberate preparation of well-defined metal oxide stepped surfaces is for UO_2(111) miscut by 11.4° to produce a repeat terrace of four uranium ions along the ⟨010⟩ direction.[11] More recent studies have appeared for vicinally cut TiO_2(110)[12,13] and TiO_2(100)[14] and for the related system $SrTiO_3$(100),[15,16] with step analysis primarily by low-energy electron diffraction (LEED) and scanning tunneling microscopy (STM). Naturally occurring, but isolated, ⟨010⟩ step defects have been observed on cleaved NiO(100) surfaces imaged with STM and atomic force microscopy (AFM) in air[17−19] and with grazing incidence X-ray scattering (GIXS).[20] These step orientations also have been modeled theoretically with static lattice simulations.[21−23]

Auger electron spectroscopy (AES) was used primarily to monitor surface cleanliness and surface stoichiometry, while X-ray photoelectron spectroscopy (XPS) provided additional information about the chemical environment of the elements present at the surface. The stepped and nonstepped substrates show characteristic binding energies and satellite structures for stoichiometric NiO in the XPS O 1s and Ni 2p peaks.[24−26] LEED was used to determine the surface crystal structure and substrate surface order. The nonstepped LEED patterns are well-defined with a characteristic (1 × 1) pattern,[27,28] while the stepped surfaces show characteristic spot-splitting in this pattern, with the maximum distance between the split-spots corresponding to the distance of a six-atom and a seven-atom terrace.

Bromobenzene adsorption studies were then carried out on vicinal NiO substrates and were compared to the nonvicinal parent NiO substrate to probe the surface reactivity. Halogenated hydrocarbons have been used to produce hydrocarbon−substrate complexes believed to be key intermediates in catalytic surface properties.[29−31] Mechanisms of halocarbon interactions with metal oxides are, themselves, also important to a variety of heterogeneous phenomena, including those involved in catalytic environmental applications,[32] in the adsorption of halocarbon pollutants on minerals and clays,[33] and in the development of a halogen "sink" on oxide surfaces. Bromobenzene is a convenient probe of metal oxide reactivity because it contains a moderately reactive aromatic-halogen bond, the cleavage of which results in easily detectable bromine, or a small number of potential bromine-containing reaction products. The carbon−carbon and carbon−hydrogen bonds, on the other hand, require much stronger interaction with the substrate for cleavage to occur. The difference in the surface reactivity between the nonstepped and stepped NiO surfaces is determined using the bromobenzene molecule, which will be shown below.

Temperature-programmed desorption (TPD) experiments provided information about the mechanism and kinetics of

* Corresponding author. E-mail: mlangell@unlserve.unl.edu.

10.1021/jp053834i CCC: $33.50
Published on Web 12/23/2005

desorption of the adsorbed bromobenzene on the nonstepped and stepped NiO surfaces. In the TPD data, bromobenzene shows a molecularly adsorbed monolayer species at 169 K for the nonstepped surface and 180 K for the stepped surfaces with a multilayer adsorbate state desorbing over the range of 174−188 K with increased exposures. An additional surface adsorbate species, only observed on the stepped surfaces, desorbed at 145 K through two different pathways, depending upon surface coverage. At low coverages, the dehalogenation/hydrogenation species, benzene, desorbs at 145 K, and no parent bromobenzene is detected co-desorbing from the surface at this temperature. At 85% monolayer saturation coverage, dehalogenation ceases, and molecular bromobenzene is also now detected desorbing from the surface at 145 K. The residual adsorbed bromine on the NiO surfaces forms a nickel−bromide complex, determined by the Br 3p XPS.

2. Experimental Methods

The stepped NiO(100) samples were cut with a diamond saw from a single-crystal boule that was 10 mm in diameter and 40 mm long and oriented along the ⟨001⟩ direction (First Reaction, Hampton Falls, NH). The 1-mm-thick sample slices were oriented with back Laue diffraction at 9.46 ± 0.25 and 8.13 ± 0.25° relative to the (100) surface plane, producing a six-atom and a seven-atom terrace-stepped surface, as confirmed by LEED analysis. Once oriented, the samples were chemical mechanical polished (CMP) in-house on a South Bay Technology lapping wheel with successively smaller grits of 14.5−0.3 μm of aluminum oxide paste (ultrapure spectrophotometric grade Al_2O_3, white glycerin, and distilled water) to a mirror finish. Two different nonstepped NiO(100) substrates also were studied. One NiO(100) sample, obtained commercially (First Reaction, Hampton Falls, NH), was a 10 × 10 × 2 mm disk and oriented along the ⟨001⟩ direction. This (100) surface was professionally CMP prepared to a mirror finish (Surfacenet GmbH, Rheine, Germany) with no further orienting or polishing in-house. The second nonstepped sample was cut and polished from the same single-crystal boule as the stepped samples by similar procedures and was found to exhibit comparable surface properties to the commercially obtained nonstepped NiO(100) substrate.

The stepped and nonstepped NiO(100) samples were individually mounted on a 304-stainless steel backing plate machined to the diameter of the crystal with the sides cut into a concave shape to ensure only the crystal surface was being monitored during experiments. Two strips of 0.0127-mm-thick tantalum foil (Alfa Aesar, 99.5%) held the NiO(100) sample in place and were spot-welded at the top and bottom of the backing plate with care taken to make sure minimal sample surface face area was covered. The sample was supported by two tantalum wires of 0.25 mm diameter (Alfa Aesar 99.9%) spot-welded to the top and bottom edge of the stainless backing plate and used to suspend the sample between the two sample mount posts. The tantalum wires also were used to resistively heat and conductively cool the sample over a temperature range of 120−850 K with provisions for cooling through an open-cycle liquid-nitrogen cryostat. A chromel−alumel, type-K, thermocouple of 0.127 mm diameter (Omega) was spot-welded to the center of the stainless steel backing plate to monitor the sample temperature.

After introduction to ultrahigh vacuum (UHV) (base pressure $\approx 3 \times 10^{-8}$ Pa), the sample was cleaned using cycles of Ar^+ sputtering (4×10^{-3} Pa Ar, 2 kV, 1.5 μAmps/cm^2) for 20 min at room temperature, then O_2 (6.6×10^{-5} Pa) annealing for 15 min at 550 K, followed by annealing under UHV for 10 min at 550 K and 10 min at 800 K. The cleanliness and stoichiometry of the sample were determined by AES. AES spectra were obtained using a Physical Electronics (Φ) 15−255G double-pass cylindrical mirror analyzer (DPCMA) with a 2 kV primary electron beam, at 50 ms per step with a scan rate of 1 eV/s signal averaged for 10 scans. The sample was considered clean when contaminants were below the level of AES detection and the O KL_2L_2 (510 eV)/Ni $L_3M_{4,5}M_{4,5}$ (848 eV) intensity ratio was 2.5 ± 0.1 for the N(E) vs E spectrum (2.2 ± 0.1 for peak-to-peak ∂N(E)/∂E spectrum), in agreement with results from previous studies on well-defined, stoichiometric NiO(100) single-crystal substrates.[7,8]

XPS data were acquired with an Al Kα photon source ($h\nu$ = 1486.6 eV) using a Φ 04-548 dual X-ray anode controlled by a Φ 50-096 X-ray source control/supply and a Φ 16-050 heat exchange/deionizer. The Φ 15-255G DPCMA was used to obtain XPS data with constant pass energies at 25, 50, or 200 eV/pass, as noted in the figure captions below. The Al Kα anode was the predominant excitation source used since the nickel Auger transitions found at "binding energies" of 544 and 538 eV in Mg Kα excited spectra interfere with the oxygen 1s XPS peak from the substrate. The binding energies were calibrated by setting the NiO lattice O 1s peak to 529.5 eV[7,8] for spectra analyzed after the removal of a Shirley background[34] and fitted with a minimum number of 40% Gaussian−60% Lorentzian peaks using XPSPEAK 4.1.[35]

The NiO(100) diffraction patterns were obtained using a set of Vacuum Generator (VG) Microtech four-grid LEED optics controlled by VG Microtech model 8011 electronics with a primary beam energy ranging from 65 to 165 eV, a filament current of 2.1−2.5 mA, and a 1 kV screen voltage bias. The LEED patterns were captured with an EHD kamPro02IR CCD video camera interfaced to a personal computer (PC), which operated the EE2000 Smartool software that was used to record and analyze diffraction images. The images were composites of at least 16 averaged frames. The nonstepped NiO(100) diffraction features were well-defined and showed the characteristic (1 × 1) pattern associated with unreconstructed, simple bulk termination.[26,27] Primary electron energies ranged from 86 to 150 eV for study of the six-atom terrace and 90 to 148 eV for the seven-atom terrace and showed spot-splitting in the diffraction patterns characteristic of stepped surfaces as described below. The maximal spacing as a function of voltage between split-spots corresponds to the distance of a six-atom and a seven-atom terrace for the NiO(100) plane with monatomic steps along ⟨010⟩.

Bromobenzene (C_6H_5Br, Aldrich, 99%) was dried over sodium sulfate (Na_2SO_4) for 1 h at 313 K under 20 Pa and stored under nitrogen. A 5 mL aliquot of bromobenzene was transferred to a 10 mL glass vial connected to the UHV chamber through a standard leak valve equipped with a needle doser to concentrate the bromobenzene vapor in the area of the sample surface. The aliquot was then subjected to a series of freeze−pump−thaw cycles to remove any dissolved gases and admitted through the leak valve to deliver a calibrated pressure of 4.7×10^{-4} Pa to the sample surface. The quality of the bromobenzene was monitored using a quadrupole mass spectrometer in the residual gas mode.

TPD was performed using a heating rate of 2 K/s with the linear temperature ramp supplied by an 818S PID Eurotherm controller. TPD desorption species were monitored by a UTI 100C quadrupole mass spectrometer operating at an ionizer energy of 77 eV and multiplexed by a PC-controlled program developed in-house. To minimize the detection of desorbing

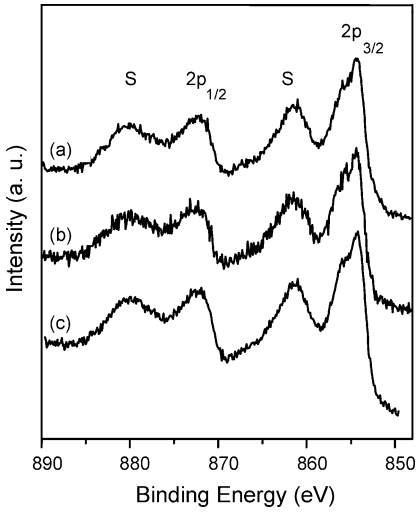

Figure 1. Ni 2p XPS spectra of (a) nonstepped NiO(100), (b) six-atom terrace-stepped NiO(100), and (c) seven-atom terrace-stepped NiO(100) acquired with Al Kα excitation source at a 25 eV pass energy.

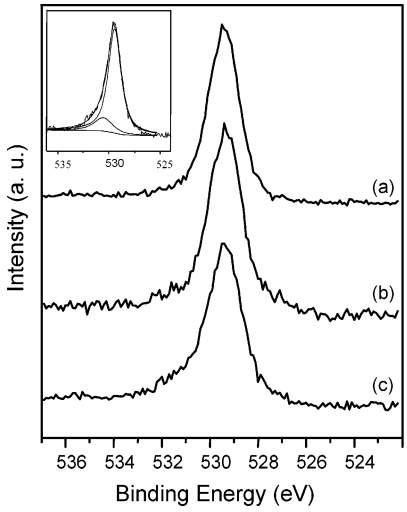

Figure 2. O 1s XPS spectra of (a) nonstepped NiO(100), (b) six-atom terrace-stepped NiO(100), and (c) seven-atom terrace-stepped NiO(100) acquired with Al Kα excitation source at a 25 eV pass energy. Inset shows spectrum C fitted with two 40% Gaussian−60% Lorentzian peaks after the removal of a Shirley background.

species from the tantalum heating wires and the sample mounting strips, the mass spectrometer ionizer was surrounded by a stainless steel shield with a 5.0 mm diameter aperture. The aperture was smaller than the exposed substrate surface, and thus prevented direct line of site to the ionizer from the tantalum and the other supporting materials. The NiO(100) substrates were dosed with bromobenzene at an initial temperature of 130 K and cleaned between exposures after each TPD experiment. Repeat dosing was used to determine uptake curves for sequential bromobenzene exposure followed by XPS, as reported below.

3. Results

The AES spectra were used primarily to monitor surface contamination and stoichiometry. The initial AES spectra for the nonstepped and stepped NiO(100) surfaces showed surface carbon contamination that was easily removed by successive cleaning cycles. Once cleaned, XPS was then used on the nonstepped and stepped NiO(100) substrates to probe the surface chemical environment. The Ni 2p XPS spectra of the nonstepped and vicinally stepped NiO(100) substrates are shown in Figure 1. XPS analysis with the current spectrometer and experimental setup probes approximately 100 Å into the near-surface region, and the effects in the XPS spectrum of five-coordinated surface terrace ions and the lower four-coordinated step edge ions are too subtle to be distinguished from the six-fold coordinated ions of the second, third, and lower NiO(100) substrate layers. The spectra in Figure 1 are characteristic of stoichiometric NiO(100) in both binding energies and satellite structure[24−26] and indicate a stoichiometric, well-oxidized surface.

The O 1s spectra for the NiO surfaces (shown in Figure 2) are fitted with two peaks, a lattice peak set in the calibration procedure to 529.5 eV[24−26] and a second peak at the higher binding energy of 530.5 eV. The second O 1s peak is at approximately 5% of the total O 1s intensity for both nonstepped and stepped NiO(100) substrates. This peak is always present and is not affected by bromobenzene adsorption. While higher binding energy peaks often are associated with surface hydroxylation of metal oxides, the value at 530.5 eV is low for hydroxyls on NiO, which are more typically reported at 531.0−531.5 eV.[36−38] Furthermore, no water or other molecular species with a hydroxyl-containing group is ever observed in the thermal desorption spectra. This second peak is likely attributed to the inaccuracies in the peak fitting procedure using Gaussian−Lorentzian peaks and background removal or possibly to a small level of surface oxygen defects[39] that are that are not completely removed in the surface preparation procedure. Both stepped and nonstepped substrates show comparable intensities and peak shapes, although there are significant differences in their reactivity to bromobenzene. The low concentration 530.5 eV peak will be further considered in the discussion section below. The binding energies of the nonstepped and stepped NiO(100) surfaces are summarized in Table 1, and are equivalent within the error of measurement.

LEED was used to examine the order and periodicity of the crystalline nickel oxide surfaces. Analyses of the diffraction patterns confirm that the substrate surfaces were well-ordered and the stepped surfaces are vicinal along ⟨010⟩ with a monatomic step height perpendicular to the (100) plane. Figure 3 shows well-ordered surface diffraction patterns for the three surfaces, and, at higher incident energies, characteristic splitting of diffraction features are shown for the two stepped surfaces. The maximum splitting energy for the six-atom terrace-stepped surface is 96 eV (Figure 3e) and 104 eV for the seven-atom terrace (Figure 3f) stepped surface. Densitometer scans of the split diffraction features are included for clarity. The EE2000 Smartool software was used to calculate the distance between the split-spot diffraction features using the NiO lattice parameter of $\mathbf{a} = 4.17$ Å[40] and to calibrate the laboratory scale distances in the LEED images to atomic distances on the NiO(100) substrate. The characteristic split-spot beam energies (E_{sp}) in eV are calculated using eq 1 at normal incidence:[41]

$$E_{sp} = \frac{(m + 0.5)^2 150}{4d^2} \quad (1)$$

where m is a positive integer, and d is the layer spacing in Å. The maximum splitting distance found for the six-atom terrace is 12.57 ± 0.2 Å, and that for the seven-atom terrace is 14.83 ± 0.2 Å, which are within the error of the calculated terrace values of 12.6 and 14.7 Å, respectively, assuming unreconstructed step termination in the lateral dimension along the step direction.

The reactivity of the nickel oxide surfaces to bromobenzene adsorption was evaluated with an uptake curve experiment. The

TABLE 1: XPS Binding Energies in eV for the Nonstepped NiO(100) Surface, the Six-Atom Terrace-Stepped NiO(100) Surface, and the Seven-Atom Terrace-Stepped NiO(100) Surface for Predosed, Bromobenzene Monolayer Saturation, and after TPD Acquired at 130 K with a 25 eV Pass Energy[a]

	Ni $2p_{3/2}$	Ni $2p_{3/2}$ satellite	Ni $2p_{1/2}$	Ni $2p_{1/2}$ satellite	O 1s	Br $3p_{3/2}$	Br $3p_{1/2}$
			flat NiO(100)				
predosed	854.4, 855.2	860.8	871.8	879.3	529.5, 530.4		
monolayer saturation	854.8, 855.7	861.4	872.3	879.4	529.5, 530.3	184.2	191.7
after TPD	854.3, 855.5	861.5	872.1	879.4	529.5, 530.3	184.6	189.6
			stepped NiO(100)				
pre-dosed, seven-atom	854.4, 855.7	861.2	872.1	879.4	529.5, 530.5		
pre-dosed, six-atom	*854.3, 855.2*	*860.8*	*872.8*	*879.3*	*529.5, 530.3*		
monolayer saturation	854.1, 855.5	860.9	872.1	879.8	529.5, 530.8	184.6	192.5
	854.4, 855.8	*861.0*	*872.2*	*879.5*	*529.5, 530.5*	*184.1*	*191.2*
after TPD	854.1, 855.5	860.9	872.1	879.8	529.5, 530.8	182.1	189.9
	854.0, 855.8	*860.1*	*872.3*	*879.4*	*529.5, 530.4*	*182.3*	*189.5*

[a]Bromine data acquired at 50 eV pass energy

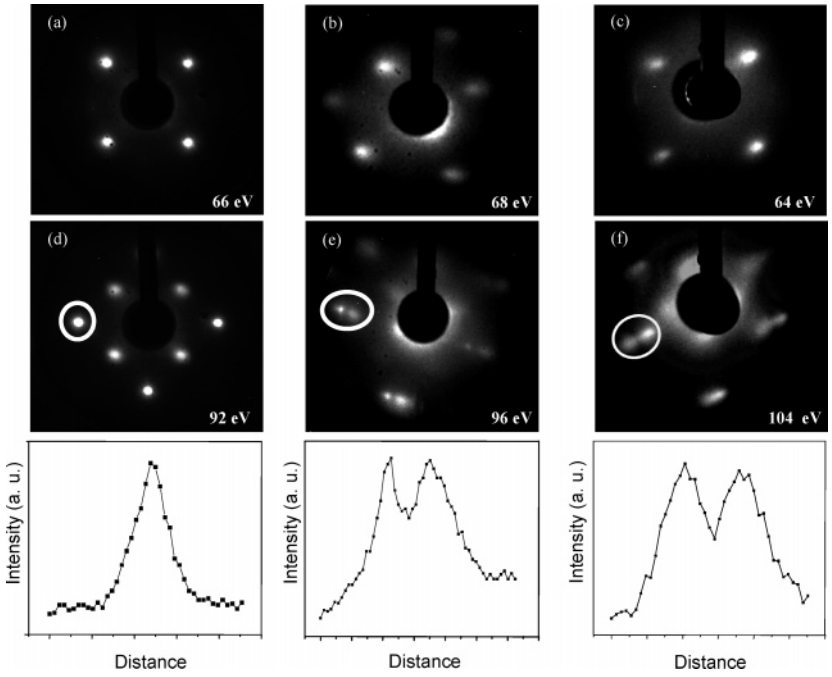

Figure 3. LEED diffraction series of the (a) nonstepped NiO(100), (b) six-atom terrace-stepped NiO(100), and (c) seven-atom terrace-stepped NiO(100), in which a−c show the maximum diffraction spot intensity and d−f show the maximum of the spot-splitting with the corresponding densitometer scan of the circled diffraction features.

C 1s and Ni 2p XPS peak intensities were used to calculate the C/Ni surface concentration ratio as a function of bromobenzene exposure. The uptake curve results are plotted for the nonstepped and the two stepped NiO(100) substrates in Figure 4. To generate this graph, XPS peak intensities were converted to C_C/C_{Ni} concentration ratios using eqs 2 and 3:[36,37]

$$\frac{I_C}{I_{NiO}} = \frac{C_C \sigma_C E_{K,Ni}{}^{1/2}}{C_{NiO}\sigma_{NiO}E_{K,C}{}^{1/2} I^{\circ}_{NiO} \exp\left(\dfrac{-d_{C6H5Br}}{\lambda_{NiO-C6H5Br}\cos\theta}\right)} \quad (2)$$

where

$$I^{\circ}_{NiO} = \sum_{n=0}^{\infty} \exp\left(\frac{-nx}{\lambda_{NiO}\cos\theta}\right) \quad (3)$$

In the above equations, I_C and I_{NiO} are the carbon 1s and nickel 2p XPS peak intensities, respectively, as determined from the fitted experimental data. The values σ_C and σ_{NiO} are the photoionization cross sections of the C1s and Ni 2p states obtained from the literature, respectively,[42] $E_{KNi}{}^{1/2}$ and $E_{KC}{}^{1/2}$ are the measured photoelectron kinetic energies for these transitions and correct for the analyzer transmission energy dependence, d_{C6H5Br} is the thickness of a bromobenzene monolayer estimated from the van der Waal radii of the constituent atoms,[43] $\lambda_{NiO-C6H5Br}$ is the mean free path of a Ni 2p electron passing through a monolayer of bromobenzene,[44] θ is the detector angle,[45] n represents successive layers into the nickel oxide substrate assuming infinite thickness with the surface layer $n = 0$, x is the distance between NiO substrate layers,[40] and λ_{NiO} is the mean free path of a Ni 2p electron passing through a nickel oxide slab of infinite thickness.[44]

Derivation and use of eqs 2 and 3 assume that electron attenuation is exponential with depth, that the bromobenzene lies with its ring parallel to or approximately parallel to the surface, and that, for the purpose of the electron attenuation of the nickel signal, the bromobenzene molecule uniformly covers the surface with an average thickness weighted by the molecular coverage. The NiO selvedge is assumed not to undergo measurable relaxation or reconstruction due to step formation

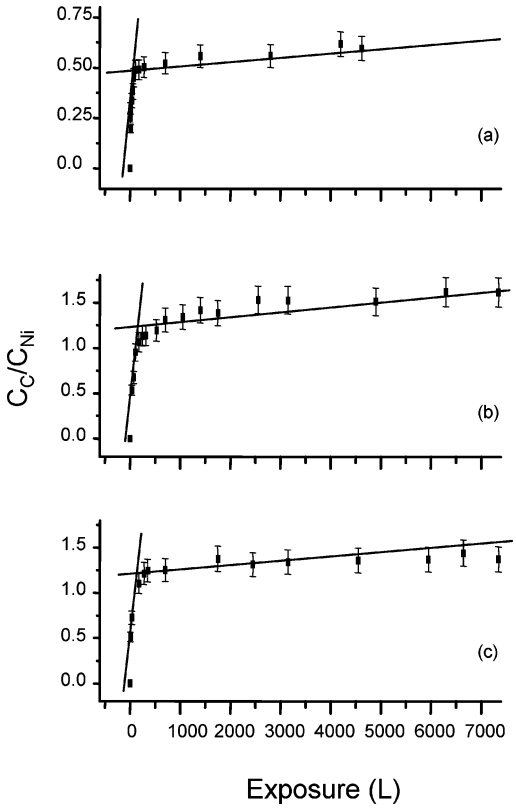

Figure 4. Uptake curve of bromobenzene at 130 K determined from the C 1s and Ni 2p XPS spectra of (a) nonstepped NiO(100), (b) six-atom terrace-stepped NiO(100), and (c) seven-atom terrace-stepped NiO(100) acquired at a 200 eV/pass energy. The intersecting lines estimate monolayer saturation. Error bars in the figure were determined to be approximately 10% of the total surface concentration because of imprecision in peak integration, and does not reflect error in dosing.

TABLE 2: Parameters Used to Calculate the Surface Concentration of C_C/C_{NiO} for Bromobenzene Exposure in the Uptake Curve Experiment

parameter	value
σ_C	1.00 (× 22 000 barns)[a]
σ_{CNi}	21.1 (× 22 000 barns)[a]
$E_{K,C}^{-1/2}$	34.67 eV
$E_{K,NiO}^{-1/2}$	25.15 eV
c_{C6H5Br}	1.95 Å[b]
x_{NiO}	4.17 Å[c]
$\lambda_{Ni-C6H5Br}$	11.5 Å[d]
λ_{NiO}	11.0 Å[d]
θ	41°[d]

[a] From ref 42. [b] From ref 43. [c] From ref 40. [d] From ref 44.

or bromobenzene adsorption and to be equal to that found in bulk NiO. The numerical values used in eqs 2 and 3 are listed in Table 2.

In the C_C/C_{NiO} uptake curve of Figure 4, the change in slope signifies the completion of the first monolayer, after which the bromobenzene is no longer adsorbing directly onto the nickel oxide substrate but onto a monolayer of adsorbed bromobenzene. Monolayer saturation was observed after 140 L (1 Langmuir = 1×10^{-6} Torr·s = 1.33×10^{-4} Pa·s) exposure for the nonstepped surface and after 280 L exposure for the stepped surfaces. The calculated concentration ratio of carbon to nickel from XPS C1s/Ni2p intensities for the first monolayer saturation coverage is $C_C/C_{NiO} = 0.509$ for the nonstepped surface and approximately 2.5 times greater for the stepped surfaces, which saturated at identical coverages ($C_C/C_{NiO} = 1.23$ for the six-atom terrace and 1.25 for the seven-atom terrace) to within the

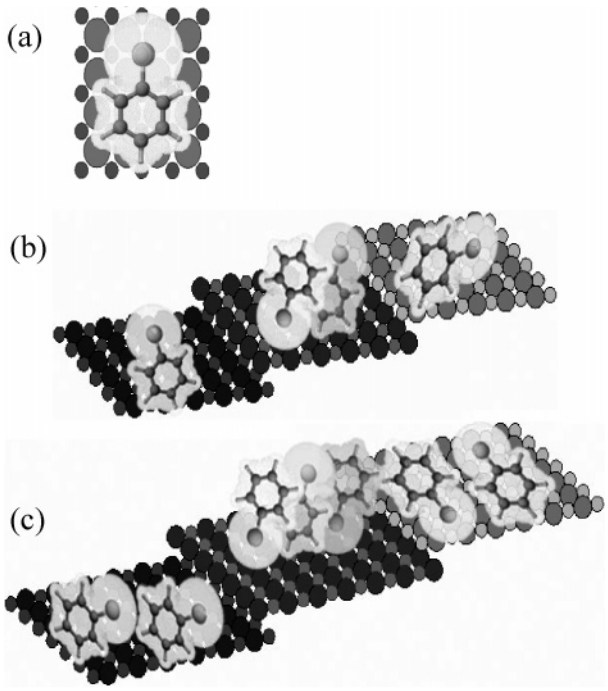

Figure 5. Schematic of bromobenzene on NiO(100) in (a) a footprint of ring-parallel orientation on the nonstepped NiO(100), (b) six-atom terrace-stepped NiO(100), and (c) seven-atom terrace-stepped NiO(100), showing their possible orientations on the step terrace, including canted orientation.

error of measurement. For the nonstepped surface, this ratio represents 0.0848 bromobenzene molecules per surface nickel atom, corresponding to one bromobenzene molecule interacting with about twelve surface nickel atoms. Including van der Waal radii, the bromobenzene molecule is approximately 9 Å long and 7.2 Å wide,[43] and closest packing arguments for bromobenzene lying parallel to a nonstepped, defect-free NiO(100) surface predict a reasonable upper limit for monolayer coverage to be about 11 surface nickel sites per bromobenzene, or a C/Ni atomic surface concentration of 0.55. The experimental atomic surface concentration for the nonstepped surface of C/Ni = 0.509 is in reasonable agreement with the value predicted by simple space-filling considerations. The molecular footprint of bromobenzene is depicted schematically for bromobenzene in Figure 5a, where the molecule is arbitrarily positioned on the surface.

On the stepped surfaces, monolayer saturation concentrations are within experimental error of each other, but are considerably higher than that of the nonstepped NiO(100) substrate. The stepped surface saturation concentration ratio of $C_C/C_{NiO} = 1.24$ corresponds to 0.207 bromobenzene molecules per surface nickel atom, or approximately one bromobenzene molecule interacting with five surface nickel atoms. The monolayer saturation coverage on the stepped surfaces is more than twice the amount that can be accommodated in a "flat" bromobenzene adsorbate geometry, even assuming a completely annealed, defect-free monolayer in which the molecules have diffused into a closest packing monolayer structure. Therefore, the packing arrangement of the bromobenzene on the stepped surfaces is quite different than that on the nonstepped surface. The only way the higher saturation coverage can be accommodated in a single monolayer is if the molecule "tilts" to present a smaller molecular footprint on the surface (Figure 5b,c).

The narrow step widths only intensify the problem of accommodating higher bromobenzene monolayer concentrations. The six-atom terrace width is approximately 12.6 Å, the

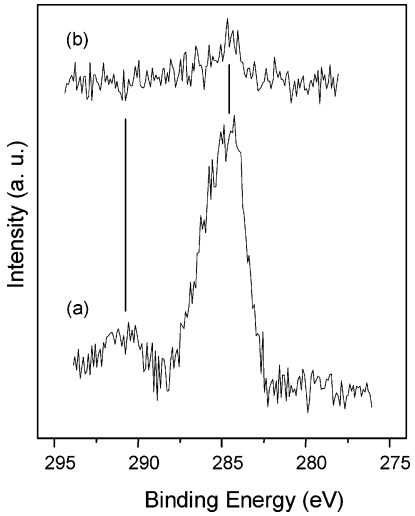

Figure 6. C 1s XPS spectra for a monolayer exposure of bromobenzene on six-atom terrace-stepped NiO(100) (a) before TPD and (b) after TPD acquired at 130 K with an Al Kα excitation source at a 50 eV pass energy.

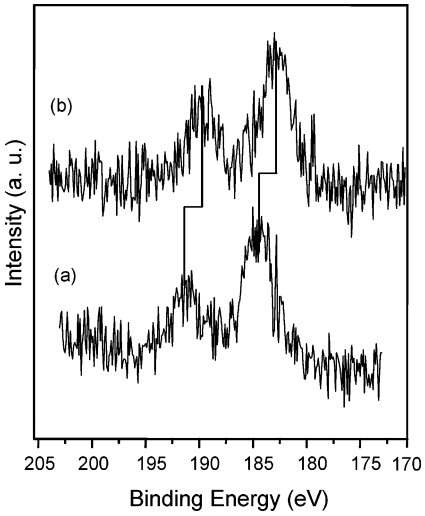

Figure 7. Br 3p XPS spectra for a monolayer exposure of bromobenzene on six-atom terrace-stepped NiO(100) (a) before TPD and (b) after TPD acquired at 130 K with an Al Kα excitation source at a 50 eV pass energy.

terrace width of the seven-atom step NiO(100) is approximately 14.7 Å, and the nonstepped parent surface terrace, resulting from the presence of random step defects, is typically within the range of 200−1000 Å.[46] In the ring-parallel adsorbate geometry, some of the surface area on the stepped NiO(100) substrates becomes unavailable for the adsorption of an adjacent molecule because it is not large enough for an additional ring-parallel molecule to fit without spilling over the step edge. Thus, the stepped surfaces can accommodate even fewer molecules at monolayer saturation coverage in a ring-parallel configuration, and the steps must induce a tilted-ring structure, shown schematically in Figure 5b,c, to explain the higher surface coverage observed on these steps.

The effect of tilted versus ring-parallel monolayer adsorbate geometry is quickly lost on subsequent layers. The bromobenzene that adsorbs in the multilayer regime is condensed bromobenzene "ice", essentially equivalent to solid bromobenzene, and appears identical on nonstepped and stepped substrates, both by XPS measurements and also as shown in the TPD data below. Even for exposures of bromobenzene greater than 4620 L, no multilayer uptake saturation is observed on any of the surfaces, as expected for the formation of condensed bromobenzene "ice".

When bromobenzene is adsorbed onto the nickel oxide surfaces at 130 K, the intensities of the bromine 3p and carbon 1s XPS spectra are always in ratios required by the stoichiometry of bromobenzene (C_6H_5Br), or in a 1/6 Br/C atomic ratio. The C 1s XPS spectra (Figure 6) show two carbon peaks, one peak for the benzene ring C−H carbons at 284.6 eV and the other 6.5 eV higher at 291.1 eV, representative of carbon bonded to the more electronegative bromine.[37] As expected, the C 1s intensity of the C−H bonded peak compared to that of the C−Br bonded peak is within the error of 5/1 and averages 4.86 ± 0.15 for the nonstepped surface, 4.91 ± 0.15 for the stepped surfaces. Bromine XPS (Figure 7 and Table 1) binding energies are also representative of bromine bonded to an aromatic hydrocarbon. Thus, the XPS data clearly show molecular adsorption of bromobenzene at 130 K.

After heating to ≥850 K, the majority of bromobenzene and its fragments have desorbed from the nonstepped NiO(100) surface. Not all of the bromobenzene desorbs cleanly. Approximately 10−15% of the monolayer carbon concentration (C/Ni ratio of 0.067 ± 0.019) remains behind as aliphatic carbon, C_xH_y, from ring fragmentation, with a C 1s binding energy of 284.6 eV and no C−Br peak detected at 291.1 eV. Residual bromine also is detected at about 15% of its original monolayer concentration (Br/Ni ratio of 0.0117 ± 0.005), and the Br 3p XPS peaks shift to lower binding energy (Table 1), indicating the formation of adsorbed bromide, Br^-_{ads}.

The stepped surfaces also show signs of residual bromobenzene adsorbate fragments, but the effect is more pronounced, and about 25% of the initial monolayer concentration remains behind as aliphatic hydrocarbon (Figure 6). A very high fraction of bromine is found after heating the stepped surface substrates to 850 K. For the six-atom terrace, 71% (Br/Ni ratio of 0.145 ± 0.005) of the initial monolayer concentration, and for the seven-atom terrace, 63% (Br/Ni ratio of 0.131 ± 0.005) is now found as surface bromide (Figure 7). The ratios of residual bromine on the two stepped surfaces are within the error of the ratio of step densities at 7/6.

Mechanisms responsible for bromobenzene desorption and decomposition were investigated by TPD. First, the nonstepped NiO(100) surface was dosed with bromobenzene with exposures ranging from 10.5 to 3620 L at 130 K. A typical subset of thermal desorption data from the nonstepped surfaces is shown in Figure 8, which depicts desorption data for the more intense C_6H_5 (AMU 77), which mirrors that of the parent C_6H_5Br TPD spectrum. Water (AMU 18) was always monitored in the multiplexing routine for the collection of all TPD data, but no H_2O was observed desorbing above the TPD background noise. There are two desorption features apparent in the nonstepped NiO(100) TPD data. The lowest energy TPD peak, found at 169 K, is attributed to the molecular desorption of monolayer bromobenzene on the substrate. The maximum desorption temperature of the monolayer peak does not vary with coverage, representative of first-order desorption kinetics.[47] Using an Arrhenius-type Polanyi−Wigner equation, known as the Redhead equation, (equation 4)[47] and the linear heating rate of 2 K/s, the activation energy of desorption is calculated:

$$-\frac{d\theta_m}{dt} = \nu_1 \theta_m \exp\left(\frac{-E}{RT_p}\right) \quad (4)$$

where θ_m is the surface coverage in molecules/cm^2, t is time in

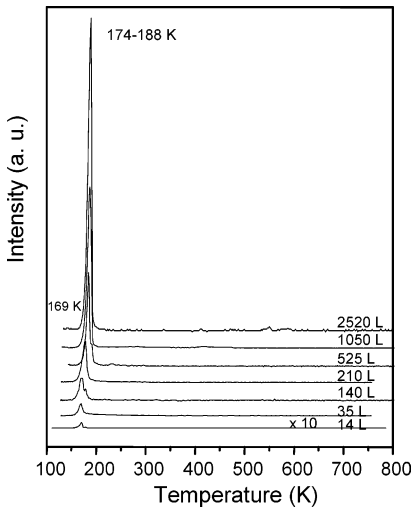

Figure 8. TPD data for the C_6H_5 (77 AMU) species from mass spectrometer ionizer fragmentation of molecularly adsorbed bromobenzene on the nonstepped NiO(100), with exposure ranging from 14 to 2520 L and dosed at 130 K.

s, ν_1 is the preexponential factor with an assumed value of 10^{13} s^{-1}, E is the activation energy of desorption in J/mol, R is the gas constant 8.314 J/mol·K, and T_p is the desorption peak temperature in K. The calculated activation energy of desorption for the molecular desorption of the monolayer peak for the nonstepped surface is 50.5 kJ/mol.

The nonstepped NiO(100) substrate sites for the monolayer species saturate after 140 L of exposure in the TPD measurement, which complements the finding of the uptake experiment. The second TPD feature, the multilayer peak, becomes visible after 105 L exposure and initially desorbs with a temperature maximum of 174 K. The desorption temperature of this feature continues to shift to higher temperatures as the coverage is increased to a final value of 188 K. This is typical kinetic behavior for condensed multilayer formation. The multilayer peak did not saturate and eventually obscures the monolayer desorption peak at sufficiently high coverages.

The stepped NiO(100) surfaces were also exposed to bromobenzene, and the results were compared to those of the nonstepped surface. The stepped surfaces were cooled to 130 K and dosed with bromobenzene over the range of 3.5−7350 L. Typical subsets of thermal desorption data from the stepped surfaces are shown in Figure 9, which depicts desorption data for the following AMUs: 78 (C_6H_6), 158 (Br_2), 156 (C_6H_5Br), and 80 (HBr). The ratios of the desorbing species were those observed for the cracking pattern of bromobenzene when gas was leaked directly into the mass spectrometer ionizer, with minor differences to be noted below. Water was also monitored, and it was not observed to desorb above the TPD background noise. There are three main desorption features in the stepped surface NiO(100) TPD data, two of which reproduce species observed desorbing from the nonstepped surface.

The highest energy TPD peak in Figure 9 is found at 180 K. This species is attributed to the molecular adsorption of the first monolayer of bromobenzene on the NiO terrace sites. The monolayer peak is about 10 degrees higher than that observed for the nonstepped surface, indicating that the adsorbate−substrate physisorbed interaction is slightly stronger on the stepped surfaces than it is on the nonstepped surface. The maximum desorption temperature also did not vary measurably with coverage, which is typical for first-order desorption kinetics. For the monolayer desorption peak at 180 K, the calculated activation energy of desorption using eq 4 and assuming the same preexponential factor (10^{13} s^{-1}) is 53.8 kJ/mol, which is 3.3 kJ/mol higher than that of the nonstepped surface. Adsorption sites for the monolayer species saturated at 280 L, which complements the results determined in the uptake curve experiment. From TPD peak intensities, the amount of bromobenzene needed for monolayer saturation on the stepped substrates is approximately double that needed to saturate the nonstepped surface.

The completion of the monolayer is best seen in Figure 10, in which TPD results are given for the most intense cracking fragment of bromobenzene, C_6H_5 (AMU 77), over a wider range of exposures from 14 to 1050 L. All features in Figure 10 mirror that of the parent C_6H_5Br TPD spectrum, as do the other cracking fragments from the molecularly desorbing bromobenzene. The second and largest peak is first observed after approximately 140 L at 174 K. This peak is attributed to multilayer desorption, which does not saturate and continues to shift to higher desorption energies with increased coverage to a final value of 188 K. The behavior of this peak and the final desorption temperature are the same as that observed on the nonstepped surface for multilayer bromobenzene "ice". Desorption from the multilayer feature eventually obscures the monolayer desorption peak.

The behavior of the lowest temperature TPD feature on the stepped surfaces, found at 145 K with submonolayer coverage,

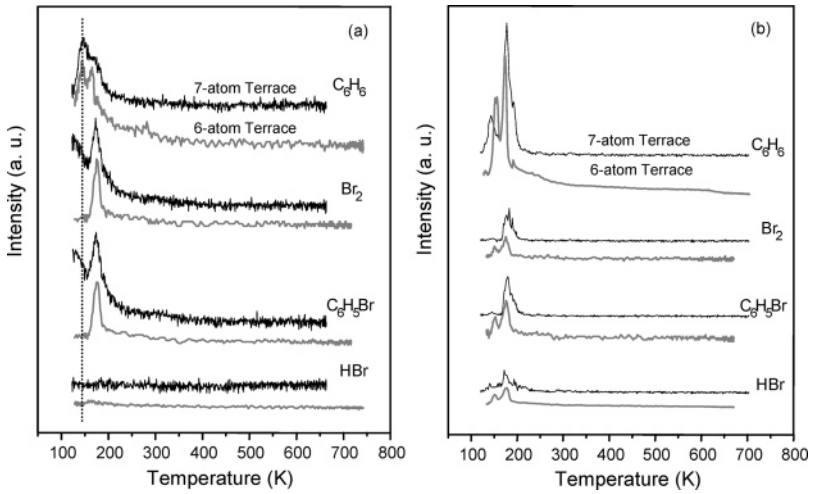

Figure 9. TPD data for the parent C_6H_5Br (156 AMU) and fragments C_6H_6 (78 AMU), Br_2 (158 AMU), and HBr (80 AMU) for the six-atom terrace and seven-atom terrace-stepped NiO(100) substrates exposed to (a) 14 L and (b) 140 L of bromobenzene at 130 K.

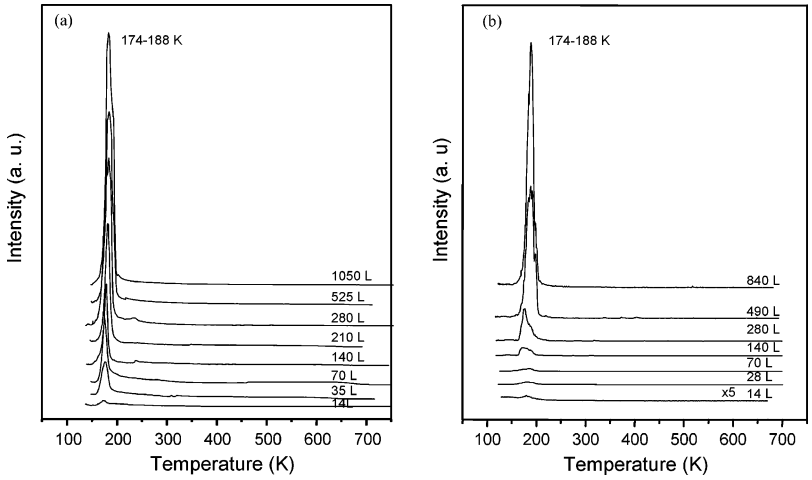

Figure 10. TPD data for the C_6H_5 (77 AMU) species of bromobenzene on the (a) six-atom terrace-stepped NiO(100), with exposures ranging from 14 to 1050 L and (b) seven-atom terrace-stepped NiO(100), with exposures ranging from 14 to 840 L dosed at 130 K.

SCHEME 1. Bromobenzene Adsorption onto NiO(100) Substrate at 130 K with Two Possible Mechanisms for Desorption: Dissociative Desorption and Molecular Desorption

is slightly more complex. This species was not observed on the nonstepped surface and is unique to the stepped substrates. At low exposures, there is no detectable molecular bromobenzene desorption from the 145 K state (14 L, Figure 9a). Rather, the debromination/hydrogenation product, benzene (C_6H_6), and its cracking fragments are found as the sole desorbing species. No bromine-containing fragments, including C_6H_5Br, HBr, and Br_2, were observed to accompany the benzene desorption from this state, indicating that the bromobenzene has dissociated and bromine from the ring−bromine bond cleavage remains behind on the nickel oxide surface. At higher exposures (for example at 140 L, Figure 9b), some bromobenzene, accompanied by its cracking fragments, begins to desorb from the stepped surfaces at 145 K, but the ratio of C_6H_6/C_6H_5Br is too high to be explained by simple fragmentation of the parent C_6H_5Br compound in the mass spectrometer ionizer. Both debromination and molecular bromobenzene desorption products are observed to desorb concurrently at 145 K, indicating a common precursor adsorbate with two possible mechanisms for desorption: one producing dissociative desorption and the other resulting in net molecular desorption, as shown in reaction mechanism 1, where the arrow (↑) following the molecule indicates desorption. At low coverages, the debromination step dominates, but this mechanism quickly saturates, indicating that dissociation must be site-limited and that the dissociation sites saturate with adsorbed bromine by monolayer coverage. The maximum peak intensity for the 145 K TPD peak is at an exposure of 240 L, an exposure that produces 85% of a monolayer. The nonstepped and stepped NiO(100) surfaces O 1s and Ni 2p photoemission peak binding energies were monitored with bromobenzene adsorption and after heating to ≥850 K during the TPD experiment. The O 1s and Ni 2p peak positions showed no detectable changes from the core substrate levels of the clean, stoichiometric NiO(100) substrate over the range of bromobenzene exposures or after TPD analysis, where bromide remained on the surface (see Table 1). The binding energy for $NiBr_2$ $2p_{3/2}$ is at 854.7 eV,[37,48] which is slightly higher than the $2p_{3/2}$ binding energy value for clean NiO at 854.4 eV. The energy difference between $NiBr_2$ and NiO is within the error of the experiment, and the difference is too small to be able to resolve the less intense signal from the nickel−bromide complex from that of the nickel oxide substrate.

4. Discussion

Bromobenzene adsorption on nonstepped and vicinally cut six-atom and seven-atom terraced stepped NiO(100) surfaces has been examined with XPS and TPD, with AES and LEED employed to measure compositional and crystallographic integrity. Bromobenzene adsorbs on all surfaces in two main states. Molecular monolayer desorption is observed at 169 and 180 K for the nonstepped and stepped surfaces, respectively, and multilayer desorption is observed from 174 to 188 K, depending upon surface coverage for all substrates. These species are well-behaved and are easily characterized by TPD and XPS.

Quantitative analysis of the XPS data for monolayer saturation coverage for the nonstepped surface yields approximately 0.509 carbon atoms for every surface nickel, which corresponds to one bromobenzene for every 12 nickel sites. This value is consistent with closest packing arguments if bromobenzene adsorbs with the aromatic ring parallel to the NiO(100) surface, which has an ideal carbon-to-nickel value of approximately 0.55. For aromatic ring adsorbate systems on transition metal oxides, the π-interactions of the aromatic ring often form the strongest adsorbate−surface interactions and result in a "flat" adsorbate structure with the benzene ring parallel to the substrate surface.[49,50] This is consistent with monolayer saturation coverages on the nonstepped NiO(100) surface, as measured by both XPS and TPD.

The monolayer saturation concentration for stepped surfaces is considerably higher and corresponds to one bromobenzene molecule for every five nickel sites. This is more than twice the carbon saturation level for monolayer adsorption on the nonstepped surface. Differences in monolayer saturation concentrations and sticking coefficients, if they exist between the two stepped surfaces, are below the detection limits of the present techniques. Step edge densities for the six-atom terraced surface are 17% higher than those for the seven-atom terraced surface, and the differences at this level are well within XPS and TPD detection limits. The similar saturation values could result from inaccessible surface areas where less than the critical adsorbate footprint is available after one bromobenzene has adsorbed onto the terrace sites. Alternatively, the step edges could induce an adsorbate geometry that templates the orienta-

tion of subsequent adsorbates, thus making the saturation coverage step density insensitive for relatively close spaced vicinal steps.

The large concentration of carbon detected for monolayer saturation on the stepped surfaces cannot be accommodated in the planar bonding configuration with the aromatic ring parallel to the substrate surface, but rather the molecular adsorption of bromobenzene on the stepped surfaces must be canted. The presence of steps may provide a template or "wall" for this to occur,[51] and the canted orientation of bromobenzene would then allow for a closer packing arrangement, resulting in higher monolayer saturation coverage. Canted or end-on bonding for aromatic ring compounds has been observed using surface enhanced Raman spectroscopy,[52] and high-resolution electron energy loss spectroscopy (HREELS).[53]

The model step defects on the vicinally cut NiO surfaces induce dehalogenation of bromobenzene for coverages up to 0.85 of the monolayer. Under these conditions, the dehalogenation/hydrogenation product, benzene, is observed to desorb, and a large fraction of the bromine (60−75%) remains behind on the substrate surface. The amount of residual surface bromide after heating to 850 K is in direct proportion to the step "defect" density, and eventually residual surface bromide saturates the dehalogenation sites. The saturation coverage of the dissociated bromine correlates with the step edge density, leading to the conclusion that step sites are active in bromobenzene dissociation and that the eventual fate of the dissociated bromine is associated with the step edges. After these sink sites fill up, a second species begins to desorb at 145 K and results in the formation of molecular bromobenzene.

On the nonstepped surface, a small amount of residual bromide also is observed, at about 15% of the monolayer concentration, and is most likely due to a low level of defects remaining on the surface after the surface preparation procedure. The small 530.5 eV O 1s peak required to fit the oxygen spectral range accurately might potentially be associated with the low level of residual defects. Unfortunately, there is no unique assignment that can be made for this very small peak, and, in the literature, it has been associated with surface hydroxyls,[36−38] capping oxygen adsorbates,[39] inaccuracies in peak fitting,[54] and a generic "defect" species.[28,55,56] It is impossible to eliminate surface defects totally, and there is a range of defect types that can be present and involved in bromobenzene dissociation. The mechanism and products might also vary from site to site. For example, the TPD data from nonstepped NiO(100) did not show the 145 K benzene desorption peak resulting from dehalogenation/hydrogenation that was observed on the stepped surface NiO(100) substrates, and there is no indication that this mechanism is operant for the low level and type of defects remaining after surface pretreatment procedures.

From the bromine 3p XPS, it is clear that the bromine has formed a nickel bromide on the NiO(100) surfaces.[37,48] Nickel bromide was not at any time detected desorbing from the surface over the temperature range of the TPD experiment ≥850 K. The total bromine concentration that remained on the NiO(100) surface after TPD for one monolayer exposure, determined by using the Br 3p peak intensity, is 15% for the nonstepped surface and 70% on the stepped surfaces. The stepped surfaces retain almost five times more adsorbed bromine than the nonstepped surface, further confirming that the amount of surface defects is directly proportional to the amount of dehalogenation and retention bromine on the surface, and that the defects are the more reactive surface sites.[51] From a catalytic and/or a halogenated aromatic compound removal perspective, the increased reactivity of the stepped surfaces is an important finding for the continued development of heterogeneous and environmental applications.

5. Conclusions

Stepped substrates with six-atom and seven-atom terraces vicinally cut along the ⟨010⟩ direction were successfully prepared on single-crystal NiO(100) and were characterized using complementary surface science techniques: AES, XPS, LEED, and bromobenzene adsorption TPD. Bromobenzene interacts with the nickel oxide substrates and forms a molecularly adsorbed monolayer and multilayer adsorbate state. The monolayer state desorbs with a maximum of 169 K for the nonstepped surface and 180 K for the stepped surfaces, and the multilayer desorbs over a range of 172−188 K on both surfaces, depending upon coverage, with a 2 K/s heating rate.

Residual bromine found on the nickel oxide surfaces, forms a nickel−bromine complex as determined by the Br 3p XPS. The dehalogenation of bromobenzene is observed in the TPD data on the stepped surfaces by two competing pathways with a desorption peak at 145 K. One pathway results in dehalogenation/hydrogenation, which saturates at submonolayer coverages, where bromine is adsorbed and benzene is desorbed. The other pathway results in molecular desorption of bromobenzene, but is only observed in significant amounts when the dehalogenation pathway is saturated. The amount of dehalogenation of bromobenzene correlates with the concentration of surface defects. The stepped surfaces retained almost five times more adsorbed bromine than the nonstepped surface, further supporting that the amount of dehalogenation and retention bromine on the surface is proportional to the number of surface defects.

Acknowledgment. We gratefully acknowledge support from the NSF under grant CHE-0213320, the Nebraska Research Initiative, and the University of Nebraska Center for Materials Research and Analysis.

References and Notes

(1) Henrich, V. E. *Chem. Phys. Solid Surf.* **2001**, *9*, 1−34.
(2) Chong, S. V.; Idriss, H. *J. Vac. Sci. Technol.* **2001**, *19*, 1933−1937.
(3) Hebenstreit, E. L. D.; Hebenstreit, W.; Geisler, H.; Ventrice, C. A.; Sprunger, P. T.; Diebold, U. *Surf. Sci.* **2001**, *486*, L467−L474.
(4) Do, T.; McIntyre, N. S.; van der Heide, P. A. W. *Surf. Sci.* **1999**, *433−435*, 765−769.
(5) Kendelewicz, T.; Liu, P.; Brown, G. E., Jr.; Nelson, E. J.; McCarthy, M. I.; Chambers, S. A. *Mineral. Mag.* **1998**, *62*, 763−764.
(6) Chusuei, C. C.; Lai, X.; Luo, K.; Goodman, D. W. *Top. Catal.* **2001**, *14*, 71−83.
(7) Weiss, W.; Somorjai, G. A. *J. Vac. Sci. Technol., A* **1993**, *11*, 2138−2144.
(8) Lad, R. J.; Antonik, M. D. *Ceram. Trans.* **1991**, *24*, 359−366.
(9) Liang, Y.; Gan, S.; Chambers, S. A.; Altman, E. I. *Phys. Rev. B* **2001**, *63*, 235402/1−235402/7.
(10) Jones, F. H.; Egdell, R. G.; Brown, A.; Wondre, F. R. *Surf. Sci.* **1997**, *374*, 80−94.
(11) Ellis, W. P.; Schwoebel, R. L. *Surf. Sci.* **1968**, *11*, 82−98.
(12) Onishi, H.; Aruga, T.; Iwasawa, Y. *J. Catal.* **1994**, *146*, 557−567.
(13) Murray, P. W.; Leibsle, F. M.; Fisher, H. J.; Flipse, C. F. J.; Thornton, G. *Surf. Sci.* **1994**, *321*, 217−228.
(14) Murray, P. W.; Leibsle, F. M.; Muryn, C. A.; Fisher, H. J.; Thornton, C. F. J. *Phys. Rev. Lett.* **1994**, *72*, 689−692.
(15) Haage, T.; Habermeier, H.-U.; Zegenhagen, J. *Surf. Sci.* **1997**, *370*, L158−L162.
(16) Brookes, N. B.; Quinn, F. M.; Thornton, G. *Vacuum* **1988**, *38*, 405−408.
(17) Imaduddin, S.; Lad, R. J. *Surf. Sci.* **1993**, *290*, 35−44.
(18) Bonnell, D. A. *Prog. Surf. Sci.* **1998**, *57*, 187−252.
(19) Castell, M. R.; Dudarev, S. L.; Muggelberg, C.; Sutton, A. P.; Briggs, G. A. D.; Goddard, D. T. *J. Vac. Sci. Technol., A* **1998**, *16*, 1055−1058.

(20) Renaud, G. *Surf. Sci. Rep*. **1998**, *32*, 1−90.
(21) Yan, M.; Chen, S. P.; Mitchell, T. E.; Gay, D. H.; Vycs, S.; Grimes, R. W. *Philos. Mag. A* **1995**, *72*, 121−138.
(22) Briquez, S.; Lakhlifi, A.; Picaud, S.; Giradet, C. *Chem. Phys.* **1995**, *194*, 65−80.
(23) Tasker, P. W.; Duffy, D. M. *Surf. Sci.* **1984**, *137*, 91−102.
(24) Shen, Z.-X.; Shih, C. K.; Jepsen, O.; Spicer, W. E.; Lindeau, I.; Allen, J. W. *Phys. Rev. Lett.* **1990**, *64*, 2442−2245.
(25) Wulser, K. W.; Hearty, B. H.; Langell, M. A. *Phys. Rev. B* **1992**, *46*, 9724−9731.
(26) Wulser, K. W.; Langell, M. A. *Surf. Sci.* **1994**, *314*, 385−397.
(27) Netzer, F. P.; Prutton, M. *J. Phys. C* **1975**, *8*, 2401−2412.
(28) Lagally, M. G. *Chem. Phys.* **1982**, *20*, 281−313.
(29) Jenks, C. J.; Bent, B. E.; Bernstein, N.; Zaera, F. *J. Phys. Chem. B* **2000**, *104*, 3008−3016.
(30) Jenks, C. J.; Bent, B. E.; Zaera, F. *J. Phys. Chem. B* **2000**, *104*, 3017−3027.
(31) Scoggins, T. B.; White, J. M. *J. Phys. Chem. B* **1999**, *103*, 9663−9672.
(32) Decker, S. P.; Klabunde, J. S.; Khaleel, K. A.; Klabunde, K. J. *Environ. Sci. Technol.* **2002**, *36*, 762−768.
(33) Estes, T. J.; Vilker, V. L *J. Colloid Interface Sci.* **1989**, *133*, 166−175.
(34) Shirley, D. A. *Phys. Rev. B* **1972**, *5*, 4709−4717.
(35) Kwok, R. W. M. *XPSPEAK 4.1*. Available for download at http://phy.cuhk.edu.hk/∼surface/XPSPEAK/.
(36) Wagner, C. D.; Riggs, W. M.; Davis, L.; Moulder, J. F. *Handbook of X-ray Photoelectron Spectroscopy*; Physical Electronics Industries: Eden Prairie, MN, 1979.
(37) Briggs, D.; Seah, M. P. *Practical Surface Analysis*, 2nd ed.; John Wiley and Sons: New York, 1990; Vol. 1.
(38) Cappus, D.; Xu, C.; Ehrlich, D.; Dillmann, B.; Ventrice, C. A., Jr.; Al Shamery, K.; Kuhlenbeck, H.; Freund, H.-J. *Chem. Phys.* **1993**, *177*, 533−546.
(39) Chambers, S. A. *The Chemical Physics of Solid Surfaces*; Elsevier Science: New York, 2001.
(40) Samsonov, G. V. *The Oxide Handbook*; IFI/Plenum: New York, 1973.
(41) Hoogers, G.; King, D. A. *Surf. Sci.* **1993**, *286*, 306−316.
(42) Scofield, J. H. *J. Electron Spectrosc. Relat. Phenom.* **1976**, *8*, 129−137.
(43) Huheey, J. E.; Keiter, E. A.; Keiter, R. L. *Inorganic Chemistry Principles of Structure and Reactivity*, 4th ed., HarperCollins College Publishers: New York, 1993.
(44) Penn, D. R. *J. Electron Spectrosc. Relat. Phenom.* **1976**, *9*, 29−40.
(45) Langell, M. A.; Berrie, C. L.; Nassir, M. H.; Wulser, K. W. *Surf. Sci.* **1994**, *320*, 25−38.
(46) Hosoi, H.; Sueoka, K.; Hayakawa, K.; Mukasa, K. *Appl. Surf. Sci.* **2000**, *157*, 218−221.
(47) Redhead, P. A. *Vacuum* **1962**, *12*, 203−211.
(48) Zaanen, J.; Westra, C.; Sawatzky, G. A. *Phys. Rev. B* **1986**, *33*, 8060−8079.
(49) Ngo, L. T.; Xu, L.; Grant, A. W.; Campbell, C. T. *J. Phys. Chem. B* **2003**, *107*, 1174−1179.
(50) Ramis, G.; Busca, G.; Lorenzelli, V. *J. Electron Spectrosc. Relat. Phenom.* **1993**, *64*−*65*, 297−305.
(51) Site, L. D.; Sebastiani, D. *Phys. Rev. B* **2004**, *70*, 115401−115404.
(52) Gao, P.; Weaver, M. J. *J. Phys. Chem.* **1985**, *89*, 5040−5046.
(53) Street, S. C.; Guo, Q.; Xu, C.; Goodman, D. W. *J. Phys. Chem.* **1996**, *100*, 17599−17605.
(54) Petitto, S. C.; Langell, M. A. *J. Vac. Sci. Technol., A* **2004**, *22*, 1690−1696.
(55) McKay, J. M.; Henrich, V. E. *Phys. Rev. B* **1985**, *32*, 6764−7672.
(56) Langell, M. A. *Surf. Sci.* **1987**, *186*, 323−338.